Received 7 November 2023; accepted 28 November 2023.
Date of publication 4 December 2023; date of current version 12 December 2023.

*Digital Object Identifier 10.1109/OJUFFC.2023.3338570*

# Analysis of Aberration Effects on Flow Imaging and Quantification in Echocardiography

**STEFANO FIORENTINI[1,2], SVEIN-ERIK MÅSØY[1,2], AND JØRGEN AVDAL[1,2,3] (Member, IEEE)**

[1]Department of Circulation and Medical Imaging, Norwegian University of Science and Technology (NTNU), 7491 Trondheim, Norway
[2]Centre for Innovative Ultrasound Solutions (CIUS), 7491 Trondheim, Norway
[3]Department of Health Research, SINTEF Digital, 7031 Trondheim, Norway

CORRESPONDING AUTHOR: S. FIORENTINI (stefano.fiorentini@ntnu.no)

This work was supported by the Centre for Innovative Ultrasound Solutions (CIUS), a Centre for Research based Innovation Appointed by the Norwegian Research Council.

This work involved human subjects or animals in its research. The authors confirm that all human/animal subject research procedures and protocols are exempt from review board approval.

**ABSTRACT** In medical ultrasound, aberration is a phenomenon that causes distortion of the ultrasound wavefront as it travels through an inhomogeneous medium. Aberration has been investigated since the 1960s and is known as a major cause of image quality loss in several applications, such as abdominal, breast, transcranial, and cardiac imaging. In the attempt to improve image quality in the presence of aberration, research has focused on two fronts: to provide deeper understanding of the physics behind aberration, and to develop robust methods for aberration correction based on such knowledge. However, most of the work found in the literature is focused towards improving BMode image quality, whereas little attention is given to other modalities. The aim of this work is to investigate the effects of aberration on two established blood flow imaging and quantification modalities, Pulsed Wave (PW) Doppler and Color Flow. The study was carried out on phantom and *in-vivo* recordings, using acquisitions and aberration conditions commonly encountered in cardiac imaging. In this work, aberration was modeled as a near-field phase screen, allowing for easier design and manufacturing compared to more realistic models. The results indicate that, as in BMode imaging, aberration degrades signal-to-noise ratio and resolution. Moreover, the increased sample volume size can significantly affect mean velocity and variance estimates in Color Flow, especially in the presence of strong velocity gradients occurring laterally to the beam direction. Similar effects were observed in PW Doppler. The conclusion is that blood flow imaging and quantification modalities in cardiac applications can potentially benefit from the development of aberration correction methods.

**INDEX TERMS** Beamforming, blood flow imaging, Color Flow, aberration.

## I. INTRODUCTION

IN MEDICAL ultrasound imaging, aberration is the distortion of the wavefront as it propagates through media with variable attenuation and speed of sound. Unless corrected for, aberrations are known to cause degradation of image quality in several applications, such as abdominal, breast, transcranial, and cardiac imaging. One of the main causes of degradation in image quality is the distortion of the Point Spread Function (PSF) caused by aberration. Increased main lobe width causes a loss of resolution, increased sidelobe levels leads to lower contrast, and weaker amplitudes reduce sensitivity.

Wavefront distortion due to refraction in the skull was documented in 1968 [1]. Subsequently, it was observed and characterized in a variety of tissue structures, such as liver and kidney [2], liver and brain [3], breast [4], [5], abdominal wall [6], [7], [8], [9], and chest wall [10]. The influence of aberrations on the statistical properties of ultrasound speckle was investigated in [11] and [12], and early approaches to aberration correction were proposed by O'Donnell and Flax [13], [14], [15]. Subsequent studies have focused on refining aberration correction methods [16], [17], [18], [19], [20] and improving the description of aberration models [21], [22], [23]. The effect of aberrations on compounding of consecutive ultrasound images was investigated in [24]. Finally, a real-time implementation of an aberration correction algorithm was recently proposed and evaluated in a set of 116 2-D Duplex recordings from 22 patients [25].

**TABLE 1. B-Mode and Color Flow acquisition parameters.**

| Parameter | Value |
|---|---|
| B-Mode frequency (Transmit/Demodulation) | 1.5 MHz/3.0 MHz |
| Color Flow frequency (Transmit/Demodulation) | 2.1 MHz/2.1 MHz |
| Color Flow sample volume | 1 mm |
| Color Flow Pulse Repetition Frequency (PRF) | 4.5 kHz |
| PW Doppler frequency (Transmit/Demodulation) | 2.0 MHz/2.0 MHz |
| PW Doppler sample volume | 5 mm |
| PW Doppler Pulse Repetition Frequency (PRF) | 5 kHz |

Most of the research in literature focused on developing aberration correction algorithms in BMode imaging, with only a few studies investigating the effects on Color Flow and spectral Doppler. The first studies investigated the effects of refraction using analytical models [26]. In [27], effects of refraction were further investigated considering the interposition of layers with different speed of sound and taking into account errors in the assumed speed of sound both in blood and tissue. A few studies tried to use the changing speckle pattern arising from moving blood cells to design new aberration correction methods. In [28] and [29] the authors used the difference between consecutive sample volume interrogations to define image quality metrics to be used in an aberration correction algorithm. In [30] and [31] instead, information from moving speckle in blood flow was used in an iterative time-reversal aberration correction algorithm, resulting in improvements in both power Doppler and BMode images.

Several studies on aberration correction for transcranial flow imaging and quantification have been presented. In [32] and [33], the aberration correction method proposed in [13] was applied to 3D transcranial Doppler imaging using contrast agents, and shown to yield increased flow detection rate and a decrease in variance. Another aberration correction method for the same application was assessed in [34], yielding increased signal level and blood flow detection rate in a clinical feasibility study.

The purpose of this work is to investigate the effects of phase aberration in Color Flow Imaging (CFI) and Pulsed Wave (PW) Doppler, with focus on cardiac applications. The analysis is performed using simulations, flow phantom recordings and *in-vivo* recordings. Aberration was induced by adding delay errors to elements and using in-house phase screens, manufactured according to a near-field phase screen model.

The paper is structured as follows. In Section II the design and manufacture of the phase screen is presented, along with the description of the simulation, flow phantom and *in-vivo* acquisition protocols. The results are presented in Section III and discussed in Section IV. Section V concludes the paper.

## II. METHODS

### A. PHASE SCREEN DESIGN AND MANUFACTURING

A phase screen based on the near-field aberration model [14] was designed in MATLAB (R2022b, The Mathworks, Natick, USA) by low-pass filtering 2D white Gaussian noise with a Gaussian low-pass kernel. The standard deviation of the Gaussian kernel was chosen to ensure that the 2D autocorrelation of the phase screen achieved 2.5 mm Full Width Half Maximum (FWHM). Two phase screens of different strength were generated by scaling the same white noise realization to achieve 45 ns and 75 ns Root Mean Square (RMS) delay, respectively, while keeping the filter specification unchanged. The FWHM and RMS values used in this study are based on *ex-vivo* chest wall measurements reported in [10]. Finally, non-zero mean phase screens were produced by subtracting the minimum delay error from the distribution, resulting in non-negative delay errors.

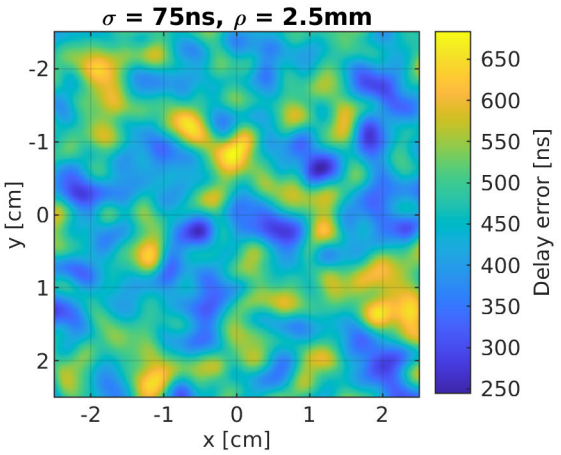


**FIGURE 1. Depiction of a non-zero mean, 75 ns RMS delay, 2.5 mm correlation length phase screen. The design process is described in Section II-A.**

Physical copies of the phase screens were manufactured using the following procedure: First, the phase screen was inverted (i.e. the peaks became valleys) and converted to thickness values using the following formula

$$\Delta z = \Delta t \frac{c_0 - c_a}{c_0 c_a} \tag{1}$$

where $\Delta t$ is the delay error, $c_0$ is the speed of sound in the medium assumed in the beamformer (1540 m/s), and $c_a$ is the speed of sound in the phase screen material. In a second step, the thickness profile was used to manufacture a mold using a high-resolution, stereo lithography (SLA) printer. An extra 0.25 mm thick layer was added at the base to support the silicone aberrator. Finally, the mold was filled with a platinum cure silicone compound (Mold Star 30, Smooth-On). The speed of sound in the material $c_a$, measured using a pulse echo setup, was 1024.2 m/s. The example shown in Fig. 1 depicts the 75 ns RMS delay, 2.5 mm correlation length phase screen.

### B. POINT SPREAD FUNCTION SIMULATION

We simulated the effect of aberration on the Point Spread Function (PSF) in Field II [35]. The PSF was calculated using the geometry and impulse response of the GE HealthCare 4Vc-D matrix phased array probe (GE Vingmed Ultrasound AS, Horten, Norway). The trandscuer has an aperture of size 21.5 mm x 15.6 mm, and has a Sub Aperture Processor (SAP) structure, where element signals are pre-beamformed in the probe into 190 channels distributed over the aperture.

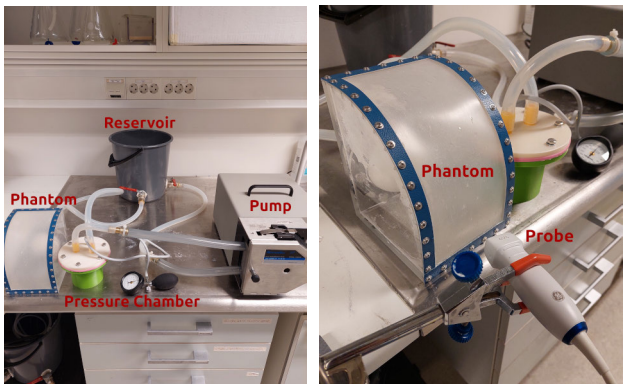


FIGURE 2. **Left panel: overview of the experimental setup. Right panel: close up view of jet phantom.**

Phase aberrations were simulated according to the near-field model described in [14]. Therefore, phase aberrations were achieved by adding a delay error at each simulated mathematical element both on transmit and receive, which was obtained from bilinear interpolation of the phase screen described in Section II-A. For the simulation, we used the non-zero mean, 75 ns RMS, 2.5 mm phase screen. To simulate a condition closer to a real acquisition using an aberration patch, a constant delay error corresponding to the aberrator base was added to all elements. The imaging parameters used in the simulations are typical of Color Flow acquisitions in echocardiography and are summarized in Table 1.

### C. JET PHANTOM RECORDINGS

Experimental data were recorded from the experimental setup shown in Fig. 2. The phantom consisted of a hemispheric dome with a 0.45 $cm^2$ circular orifice, placed in a policarbonate enclosure, and equipped with an acoustic window. A peristaltic pump (Model 77600-62, Masterflex, Avantor) was used to circulate a blood mimicking fluid, and a pressurized chamber was placed between the pump and the phantom to attenuate the oscillations induced by the pump. The blood mimicking fluid consisted of a mixture of water and corn starch in a concentration of approximately 1 g/L, which ensured fully developed speckle. The pump flow rate was set to 3.6 L/min, resulting in a maximum flow velocity of 1.5 m/s, measured using Continuous Wave (CW) Doppler.

Channel data were recorded using a GE HealthCare Vivid E95 scanner equipped with a 4Vc-D matrix phased array probe. The measurement protocol consisted of 1.5 s of 2D Duplex acquisition followed by 1.5 s of PW Doppler acquisition, with the sample volume placed at the orifice. For both sequences, three sets of recordings were performed. First without an aberrator and subsequently with the phase screens described in Section II-A. An overview of the acquisition parameters is given in Table 1.

Channel data were beamformed and post-processed in MATLAB (R2022b, The Mathworks, Natick, USA) using a library that replicates the reconstruction steps performed on the Vivid E95 scanner. Beamformed data from Color Flow acquisitions were clutter filtered. Finally, power, mean velocity, and spectral bandwidth were estimated using lag-0 and lag-1 estimators. Beamformed data from PW Doppler acquisitions were clutter filtered, and spectral analysis was performed using a Welch spectral estimator, 10 ms observation windows, Hamming windowing, and 50 % window overlap.

### D. HEALTHY VOLUNTEER RECORDINGS

Channel data were recorded from a healthy volunteer using the Vivid E95 scanner equipped with a 4Vc-D matrix phased array probe. Measurement consisted of 1.5 s of 2D Duplex acquisition from an apical four chamber (A4C) view. Channel data were beamformed and post-processed in MATLAB using a library that replicates the reconstruction steps performed on the Vivid E95 scanner. To ensure that frames processed with and without phase screen could be compared under the same view and flow regime, phase aberration was simulated by adding delay errors during receive beamforming. This means that, in contrast to using a silicone patch, phase aberration occurs only on receive and on channel data that were already prebeamformed in the SAPs. Delay errors for individual elements were obtained by bilinear interpolation from the 2D phase screen distribution described in Section II-A. The acquisition parameters are given in Table 1.

## III. RESULTS

### A. POINT SPREAD FUNCTION SIMULATION

Fig. 3 and 4 show the results from a Field II point-spread-function (PSF) simulation using the geometry and impulse response of GE HealthCare 4Vc-D, and the Color Flow acquisition parameters given in Table 1. In the upper panels, the PSF results without phase screen and with the 75 ns RMS delay, 2.5 mm correlation length phase screen described in Section II-A are compared. In the lower panels, delayed channel data, acquired from two selected beams are shown. The results indicate that the presence of a phase screen causes a distortion of the delayed IQ data and phase wrapping. This again causes undesired destructive interference, resulting in a weaker main lobe and increased side-lobe levels. The consequence of using a non-zero mean phase screen is a displacement of the PSF along the range direction, which also manifests itself as a constant time shift in the delayed channel data.

Fig. 5 shows the lateral PSF profile at focal depth. Closer inspection of the results reveals a 2.2 dB decrease in peak intensity and a 10 dB increase in sidelobe level for the 45 ns RMS delay aberrator, and a 7.9 dB decrease in peak intensity and a 10 dB increase in sidelobe level for the 75 ns RMS delay aberrator.

### B. JET PHANTOM RECORDINGS

#### 1) COLOR FLOW

In Fig. 6 blood signal power, mean velocity and bandwidth are shown for three 2D Duplex frames recorded under different phase aberration conditions. The blood signal power was segmented by thresholding 8 dB above the estimated noise floor. Histograms of the corresponding variables are shown in the lower panels, allowing quantitative comparisons. The

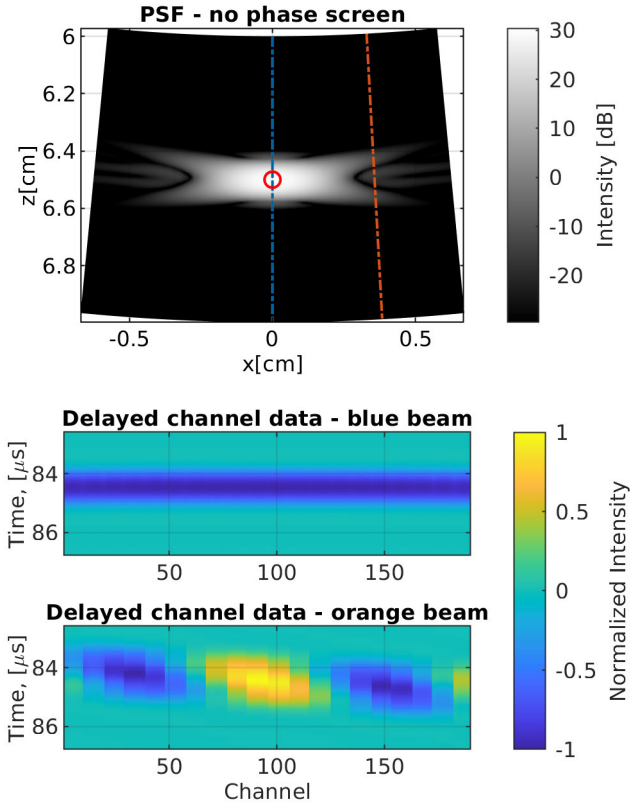


**FIGURE 3.** **Baseline PSF simulation using Field II. The lower panel displays the normalized real part of the delayed IQ channel data, acquired at the transmit beams indicated using a blue and orange dashed line in the upper panel. The point scatterer is located at the point highlighted in red.**

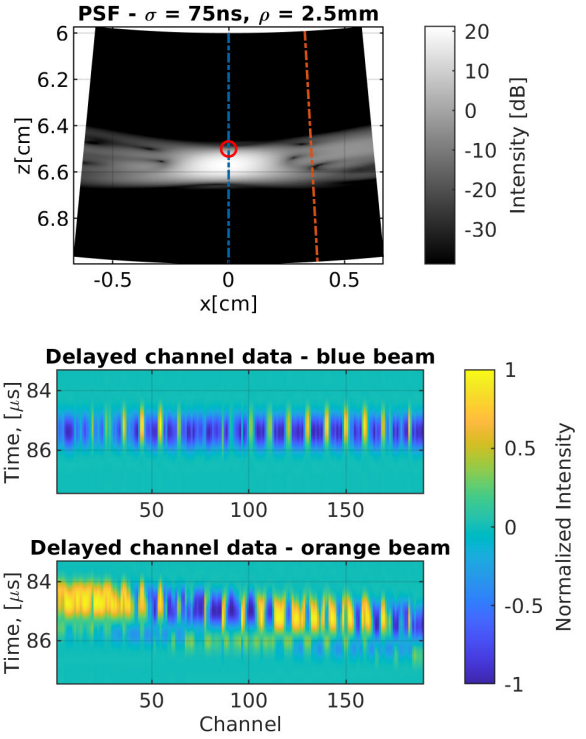


**FIGURE 4.** **Distorted PSF simulated in Field II. The lower panel displays the normalized real part of the delayed IQ channel data, acquired at the transmit beams indicated using a blue and orange dashed line in the upper panel. The point scatterer is located at the point highlighted in red.**

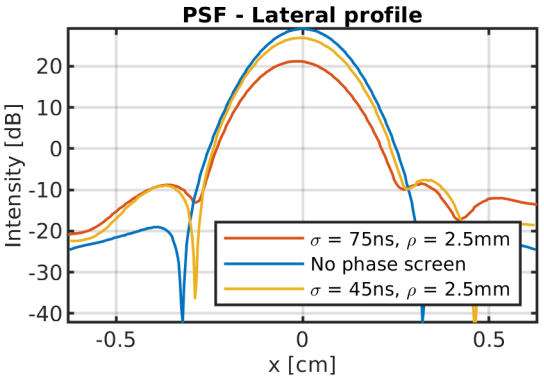


**FIGURE 5.** **Lateral PSF profiles generated without using a phase aberrator, and using the 45 ns and 75 ns RMS delay phase aberrators.**

mean signal power loss calculated from the histograms was 2.8 dB and 7.1 dB for the 45 ns and 75 ns RMS delay aberrators, respectively, corresponding well with PSF simulations shown in Fig. 5.

Visual inspection of the mean velocity estimates indicates that the interposition of a phase screen causes a decrease in the estimated mean velocity in regions with high spatial gradients, i.e. close to the jet core.

Inspection of the mean velocity histograms reveals a compression of the velocity estimates with increasing strength of the phase screen. This is confirmed by the standard deviation of the histograms, that decreases from 0.29 m/s without aberrator to 0.26 m/s and 0.22 m/s for the 45 ns and 75 ns RMS delay aberrators, respectively. On the other hand, the average of the histograms does not change significantly, being 0.57 m/s without aberrator, 0.57 m/s and 0.58 m/s with the 45 ns and 75 ns RMS delay aberrators respectively.

Inspection of the bandwidth histograms indicates that the estimated blood signal bandwidth increases with the intensity of phase aberration. This is confirmed by the mean of the histograms that increases from 0.18 without aberrator, to 0.2 and 0.25 for the 45 ns and 75 ns RMS delay aberrators, respectively. Visual inspection of the images indicates that this phenomenon occurs especially near the phantom orifice, where velocity gradients are highest.

The average number of detected pixels in each frame was 4400 without aberrator, 4600 for the 45 ns RMS delay aberrator, and 4570 for the 75 ns RMS delay aberrator, which visually translates to an apparent broadening of the jet, as shown by the increased size of the detected flow regions that extend outside of the dashed blue lines.

### 2) PW DOPPLER

Fig. 7 depicts the PW Doppler spectra recorded at the jet orifice, with and without a 75 ns RMS phase screen placed in front of the transducer. Results indicate that increased

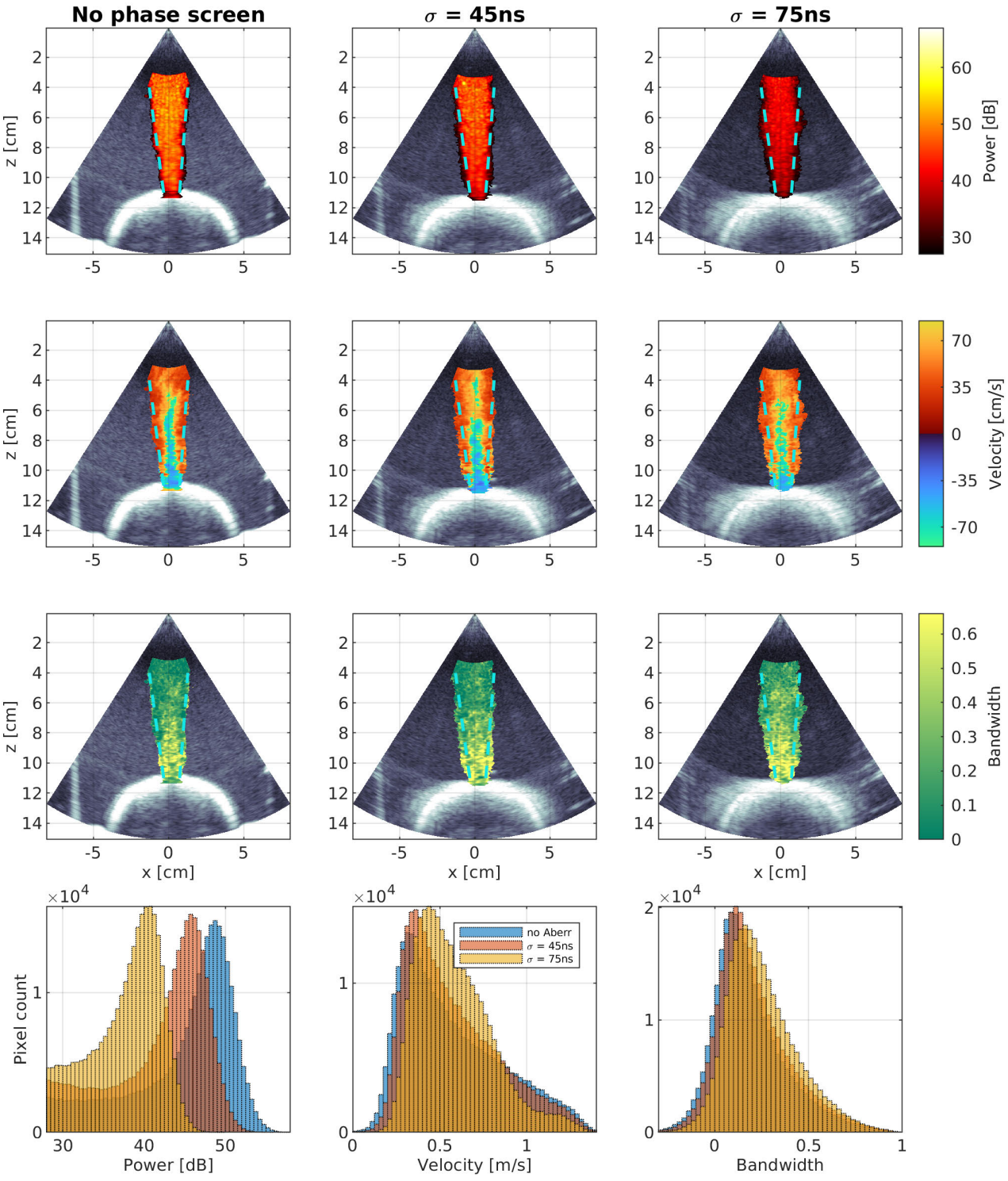


**FIGURE 6. 2D Duplex images of the jet phantom depicting power, mean velocity and bandwidth estimates from the autocorrelation estimator. The first column shows results from data acquired without phase screen, the second and third columns show results from data acquired with the silicone phase screens described in Section II-A. Color information is displayed in the pixels where signal power is 8 dB above the estimated noise floor. The dashed blue lines are provided as a reference to visually appreciate the broadening of the jet. In the last row, histograms summarize the statistics of the estimates throughout the entire acquisition.**

aberration strength causes both a loss of spectral power and a loss of definition of the peak velocities. At the same time, it is possible to notice increased signal levels at lower velocities. The lower panel depicts PW Doppler spectra

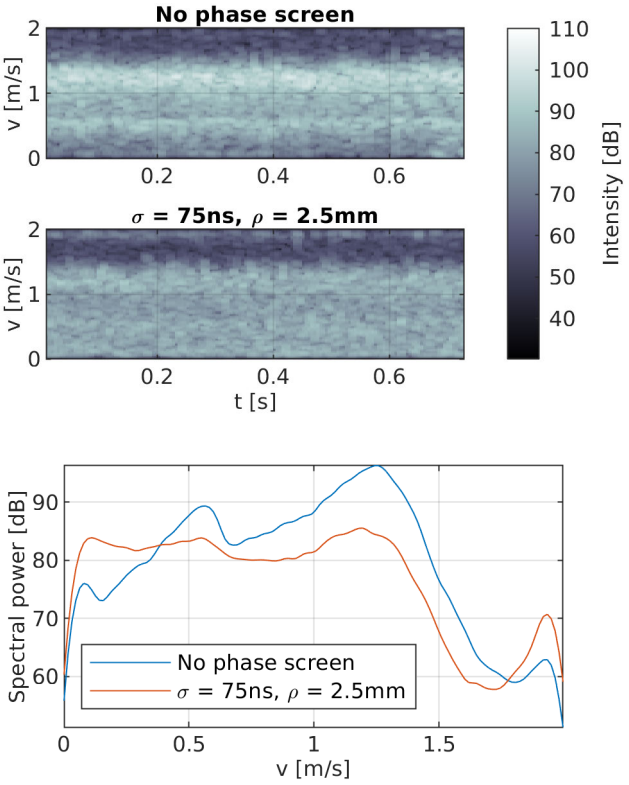


**FIGURE 7. Upper panel: PW Doppler spectra recorded from the jet phantom without phase screen and with a 75 ns RMS silicon aberrator. Lower panel: time-averaged PW Doppler spectra shown in the upper panels.**

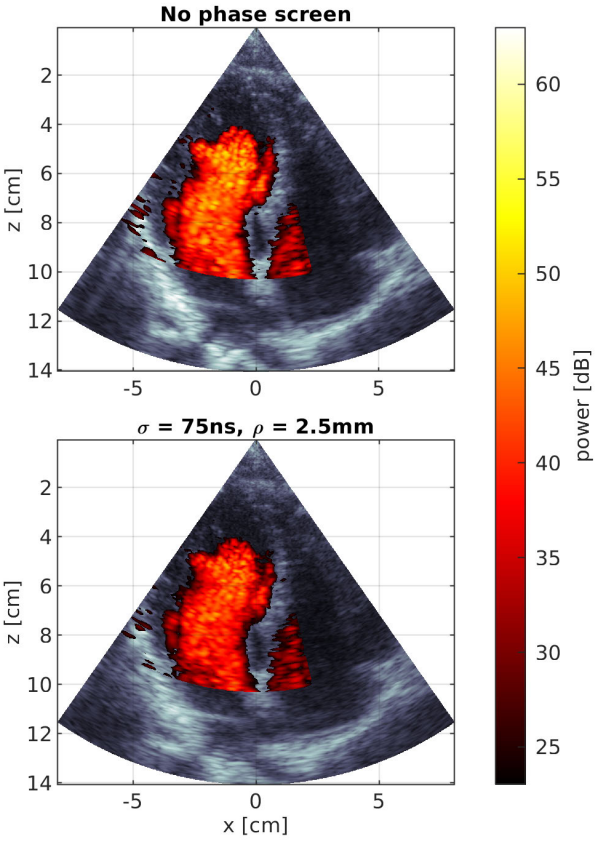


**FIGURE 8. Blood signal power estimated from a Duplex acquisition of a healthy volunteer. The figure processed without aberration is shown in the upper panel, the figure processed with phase aberration in the lower panel. Color information is displayed in the pixels where the level of blood signal is 4 dB above the estimated noise floor.**

averaged throughout the observation window. The results show that aberration causes the PW spectrum to appear more uniform, whereas there is a higher intensity close to the jet velocity in the case without aberration. Results also indicate an average 10 dB SNR loss, which is in agreement with simulation and Color Flow results.

### C. HEALTHY VOLUNTEER

In Fig. 8 the blood signal power is shown in two Duplex frames, processed from an apical four chamber acquisition of a healthy volunteer. In the lower panel, phase aberration was achieved in post-processing by injecting time delay errors during beamforming. The power of the blood signal was segmented by thresholding 4 dB above the estimated noise floor. Similarly to what shown in Fig. 6, the results indicate that phase aberration causes both a decrease in signal intensity and a loss in spatial resolution, appearing as a broadening of the segmented region, most evident along the septum wall.

In Fig. 9 the mean blood velocity estimated from lag-1 autocorrelation is shown. The results indicate that phase aberration can cause a significant change in the estimated mean velocities, especially close to the vortex center, where high velocity gradients occur along the lateral direction. In Fig. 10 the blood signal bandwidth, estimated from lag-1 autocorrelation and signal power, is displayed. Here it may be observed that phase aberration can cause a significant increase in signal bandwidth, especially close to the vortex center, where high velocity gradients occur along the lateral direction. Fig. 11 and 12 show mean blood velocity and bandwidth histograms estimated inside the blue and orange regions shown in Fig. 9 and 10. An analysis of the bandwidth histograms shows an increase of the average value from 0.14 to 0.19 in the blue region and from 0.22 to 0.24 in the orange region. An analysis of the mean velocity histograms shows an increase of the average values from 0.16 m/s to 0.21 m/s in the blue region and a decrease from 0.32 m/s to 0.31 m/s in the orange region. The standard deviation decreases from 0.32 m/s to 0.3 m/s in the blue region and increases from 0.3 m/s to 0.32 m/s in the orange region.

## IV. DISCUSSION

In this work, we have investigated the effects of phase aberrations on Color Flow and PW Doppler in cardiac applications. Results indicate that phase aberrations can potentially have a significant effect on both modalities, in terms of average signal loss and distortion of the velocity estimates. While the former may be explained by lower RMS intensity of the point spread function [11], the latter may be a consequence of the distortion of the point spread function

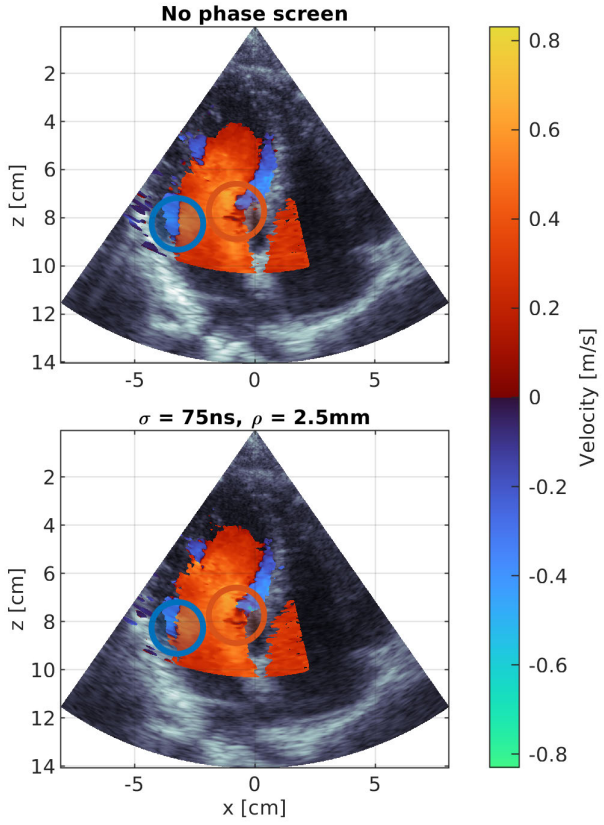


FIGURE 9. **Mean blood velocity estimated from a Duplex acquisition of a healthy volunteer. The figure processed without aberration is shown in the upper panel, the figure processed with phase aberration in the lower panel.**

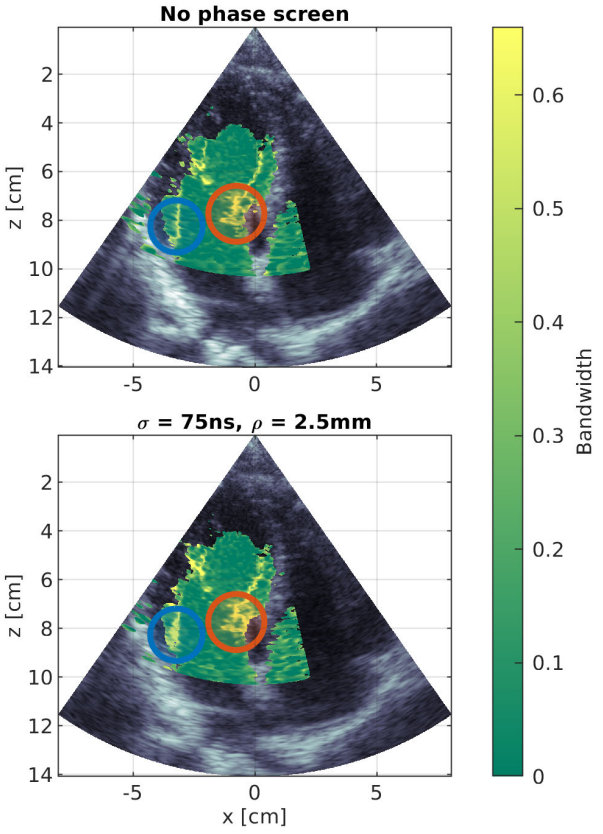


FIGURE 10. **Blood spectral bandwidth estimated from a Duplex acquisition of a healthy volunteer. The figure processed without aberration is shown in the upper panel, the figure processed with phase aberration in the lower panel.**

and increased sample volume size, causing a wider range of velocities to be picked up. This would also explain why the observed changes are more evident in regions where high velocity gradients occur laterally to the ultrasound beam.

Results from simulations and Duplex jet phantom recordings in the upper panels of Fig. 6 suggest that, as in BMode imaging, phase aberration leads to decreased power level in Color Flow and decreased resolution, resulting in an increased spatial extent of the detected blood region. This effect may be relevant in applications where quantitative assessment of jet properties is important, such as quantification of the size of the *vena contracta*, and flow rate measurements. Visual inspection also suggests that the distortion in Color Flow is not as strong as in the underlying BMode image. This result can be explained by the difference in pulse center frequency between the two imaging modalities. In previous studies [36], [37] it has been observed that higher pulse frequencies tend to be more affected by the same phase screen, as delay errors approach the wavelength.

The results in Fig. 6 also indicate a compression of the range of mean velocity estimates, and an average increase in spectral bandwidth. These two phenomena may again be explained by the combined effect of PSF distortion and increase in side-lobe levels, as shown in Fig. 5, which in turn causes a wider range of velocities to be picked up by the sample volume. The effect will be more evident in regions with strong velocity gradients along the lateral dimension.

Observations from *in vivo* results are consistent with simulations and phantom recordings. More specifically, the results shown in Fig. 8 indicate that phase aberrations cause smearing of the blood signal over the tissue region,making arbitration more challenging. The same mechanism may be used to explain changes in the estimated mean velocities and signal bandwidths, which can even result in an altered perceived flow pattern *in-vivo*. Both effects can be seen in the blue and orange regions highlighted in Fig. 9 and 10, whereas the change in mean velocity and bandwidth statistics is shown in Fig. 11 and 12.

Visual inspection of the PSFs showed in Fig. 5 indicates that the phase screen used in this study did not lead to beam steering and split beam effects, which may also occur. The implications of beam steering caused by refraction have already been investigated in previous works [26], [27]. In the latter, it was observed that the main risk that may occur is an overestimation of the mean velocity and peak velocity. The current work may be seen as complementary to these studies, documenting the effects of resolution loss in addition to the effects of beam steering. A detailed analysis of the combined effect of beam steering and beam distortion on Color Flow and spectral Doppler could be investigated in future work.

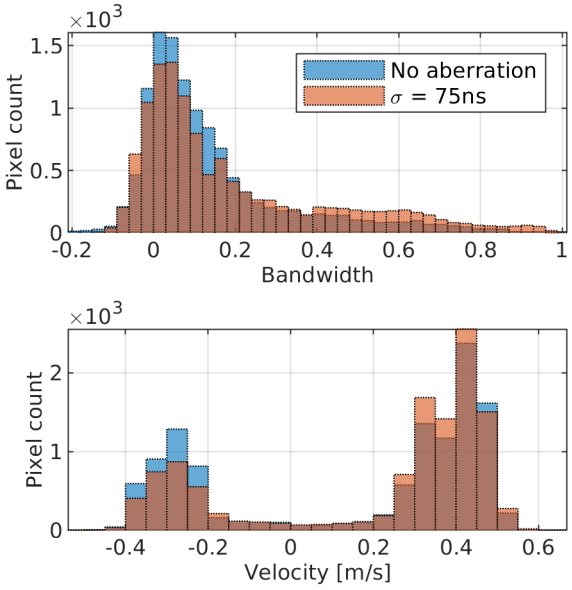


**FIGURE 11. Histograms that summarize the Color Flow estimates within the blue ROI shown in Fig. 9, and 10.**

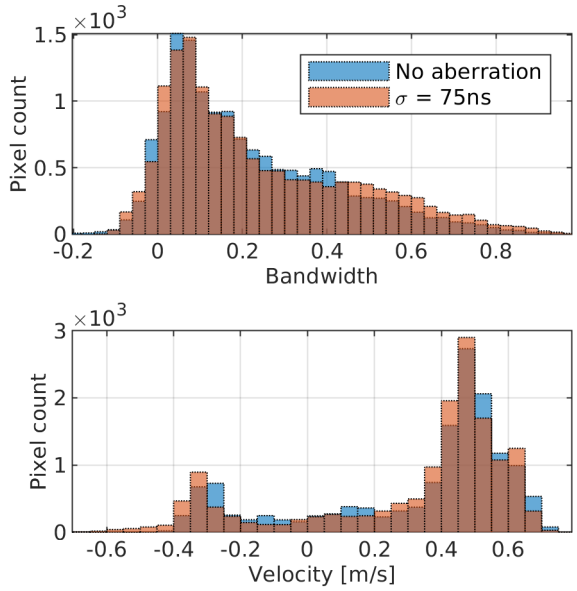


**FIGURE 12. Histograms that summarize the Color Flow estimates within the orange ROI shown in Fig. 9, and 10.**

The effects of aberration on Color Flow and PW Doppler were analyzed assuming the near-field screen aberration model described in [14]. The choice was motivated by the reduced complexity in designing and manufacturing aberrators based on this model compared to more sophisticated ones, such as the mid-field aberration model [38] and distributed models [18]. One known limitation of this model is that it only generates a single isoplanatic patch that extends over the entire imaging region. Skin, fat, muscle, and connective tissue in a patient constitute a complex inhomogeneous layer with non-negligible thickness, which results in depth- and steering-dependent phase distortion, amplitude distortion due to frequency dependent attenuation, and reverberation effects. Further work could investigate the effects of more realistic aberration models as well as the effects of aberration in other applications, such as vascular or abdominal, in which the statistical properties of the aberrator will differ. On the other hand, although the use of a simple aberration model in this work may limit the extent of validity of the quantitative results presented in this work, more accurate aberration models are not expected to deviate from the trends observed in this study.

Phase aberration in the *in-vivo* example was achieved in post-processing by adding delay errors at receive beamforming. The motivation behind this choice was to isolate the analysis of the effects of phase aberration from undesired sources of uncertainty, such as view reproducibility, beat-to-beat variations and temporal mismatch. Closer inspection of the histograms in Fig. 11 and 12 shows a more moderate increase in signal bandwidth estimates compared to *in-vitro* results, and a less predictable effect on mean velocity estimates, possibly due to the adopted strategy to induce aberrations. Acknowledging these limitations, we believe that this approach can still be useful to understand the effects of aberration on Color Flow.

## V. CONCLUSION

In this work we have investigated the effects that phase aberration can have on two established blood flow imaging and quantification modalities used in cardiac imaging, Pulsed Wave (PW) Doppler and Color Flow. The study was carried out using simulations, phantom and *in-vivo* recordings. Aberration was modeled using a near field phase screen, which allowed for easier design and manufacturing compared to more advanced and realistic models. Simulation and experimental results indicate that phase aberration degrades the signal-to-noise ratio up to 8 dB for a 75 ns RMS delay phase screen, as well as causing a compression of the range of mean velocities and an increase in the bandwidth estimated using lag-1 autocorrelation, especially in regions of strong velocity gradients. Similarly to B-Mode imaging, the experimental results also indicate a loss in resolution, signaled by an increased number of pixels above the detection threshold. Results from recordings of a healthy volunteer partially confirm these findings. Future work could investigate the effect of more realistic aberrators and the effect in different applications.

## REFERENCES

[1] D. N. White, J. M. Clark, J. N. Chesebrough, M. N. White, and J. K. Campbell, "Effect of the skull in degrading the display of echoencephalographic B and C scans," *J. Acoust. Soc. Amer.*, vol. 44, no. 5, pp. 1339–1345, Nov. 1968.

[2] R. Banjavic, J. Zagzebski, E. Madsen, and R. Jutila, "Ultrasonic beam sensitivity profile changes in mammalian tissue," in *Ultrasound in Medicine*, vol. 4. Boston, MA, USA: Springer, 1978, pp. 515–518, doi: 10.1007/978-1-4613-4021-8_117.

[3] F. S. Foster and J. W. Hunt, "Transmission of ultrasound beams through human tissue—Focussing and attenuation studies," *Ultrasound Med. Biol.*, vol. 5, no. 3, pp. 257–268, Jan. 1979.

[4] M. Halliwell, "Ultrasonic beam distortion by the normal human breast in vivo," in *Ultrasound in Medicine*, vol. 4. Boston, MA, USA: Springer, 1978, pp. 555–556, doi: 10.1007/978-1-4613-4021-8_121.

[5] L. M. Hinkelman, D.-L. Liu, R. C. Waag, Q. Zhu, and B. D. Steinberg, "Measurement and correction of ultrasonic pulse distortion produced by the human breast," *J. Acoust. Soc. Amer.*, vol. 97, no. 3, pp. 1958–1969, Mar. 1995, doi: 10.1121/1.412069.

[6] L. M. Hinkelman, D.-L. Liu, L. A. Metlay, and R. C. Waag, "Measurements of ultrasonic pulse arrival time and energy level variations produced by propagation through abdominal wall," *J. Acoust. Soc. Amer.*, vol. 95, no. 1, pp. 530–541, Jan. 1994, doi: 10.1121/1.408347.

[7] L. M. Hinkelman, T. D. Mast, L. A. Metlay, and R. C. Waag, "The effect of abdominal wall morphology on ultrasonic pulse distortion. Part I. Measurements," *J. Acoust. Soc. Amer.*, vol. 104, no. 6, pp. 3635–3649, Dec. 1998, doi: 10.1121/1.423946.

[8] T. D. Mast, L. M. Hinkelman, M. J. Orr, V. W. Sparrow, and R. C. Waag, "Simulation of ultrasonic pulse propagation through the abdominal wall," *J. Acoust. Soc. Amer.*, vol. 102, no. 2, pp. 1177–1190, Aug. 1997, doi: 10.1121/1.421015.

[9] T. D. Mast, L. M. Hinkelman, M. J. Orr, and R. C. Waag, "The effect of abdominal wall morphology on ultrasonic pulse distortion. Part II. Simulations," *J. Acoust. Soc. Amer.*, vol. 104, no. 6, pp. 3651–3664, Dec. 1998, doi: 10.1121/1.423947.

[10] L. M. Hinkelman, T. L. Szabo, and R. C. Waag, "Measurements of ultrasonic pulse distortion produced by human chest wall," *J. Acoust. Soc. Amer.*, vol. 101, no. 4, pp. 2365–2373, Apr. 1997, doi: 10.1121/1.418248.

[11] G. Trahey, "Properties of acoustical speckle in the presence of phase aberration part I: First order statistics," *Ultrason. Imag.*, vol. 10, no. 1, pp. 12–28, Jan. 1988. [Online]. Available: https://www.sciencedirect.com/science/article/pii/0161734688900636

[12] S. W. Smith, G. E. Trahey, S. M. Hubbard, and R. F. Wagner, "Properties of acoustical speckle in the presence of phase aberration Part II: Correlation lengths," *Ultrason. Imag.*, vol. 10, no. 1, pp. 29–51, Jan. 1988.

[13] S. Flax and M. O'Donnell, "Phase-aberration correction using signals from point reflectors and diffuse scatterers: Basic principles," *IEEE Trans. Ultrason., Ferroelectr., Freq. Control*, vol. 35, no. 6, pp. 758–767, Jun. 1988.

[14] M. O'Donnell, "Phase aberration measurements in medical ultrasound: Human studies," *Ultrason. Imag.*, vol. 10, no. 1, pp. 1–11, Jan. 1988. [Online]. Available: https://www.sciencedirect.com/science/article/pii/0161734688900624

[15] M. O'Donnell and S. W. Flax, "Phase-aberration correction using signals from point reflectors and diffuse scatterers: Measurements," *IEEE Trans. Ultrason., Ferroelectr., Freq. Control*, vol. 35, no. 6, pp. 768–774, Nov. 1988.

[16] D.-L. Liu and R. C. Waag, "Correction of ultrasonic wavefront distortion using backpropagation and a reference waveform method for time-shift compensation," *J. Acoust. Soc. Amer.*, vol. 96, no. 2, pp. 649–660, Aug. 1994.

[17] S. Krishnan, P.-C. Li, and M. O'Donnell, "Adaptive compensation of phase and magnitude aberrations," *IEEE Trans. Ultrason., Ferroelectr., Freq. Control*, vol. 43, no. 1, pp. 44–55, Jan. 1996.

[18] S.-E. Måso/y, T. F. Johansen, and B. Angelsen, "Correction of ultrasonic wave aberration with a time delay and amplitude filter," *J. Acoust. Soc. Amer.*, vol. 113, no. 4, pp. 2009–2020, Apr. 2003, doi: 10.1121/1.1559174.

[19] S.-E. Måsøy, B. Angelsen, and T. Varslot, "Estimation of ultrasound wave aberration with signals from random scatterers," *J. Acoust. Soc. Amer.*, vol. 115, no. 6, pp. 2998–3009, Jun. 2004.

[20] S.-E. Måsøy, T. Varslot, and B. Angelsen, "Iteration of transmit-beam aberration correction in medical ultrasound imaging," *J. Acoust. Soc. Amer.*, vol. 117, no. 1, pp. 450–461, Jan. 2005.

[21] J. C. Tillett, J. P. Astheimer, and R. C. Waag, "A model of distributed phase aberration for deblurring phase estimated from scattering," *IEEE Trans. Ultrason., Ferroelectr., Freq. Control*, vol. 57, no. 1, pp. 214–228, Jan. 2010.

[22] Y.-T. Shen, M. I. Daoud, and J. C. Lacefield, "Computational models of distributed aberration in ultrasound breast imaging," *IEEE Trans. Ultrason., Ferroelectr., Freq. Control*, vol. 57, no. 12, pp. 2627–2636, Dec. 2010.

[23] B. E. Treeby, J. Jaros, A. P. Rendell, and B. T. Cox, "Modeling nonlinear ultrasound propagation in heterogeneous media with power law absorption using a k-space pseudospectral method," *J. Acoust. Soc. Amer.*, vol. 131, no. 6, pp. 4324–4336, Jun. 2012.

[24] J. J. Dahl, D. A. Guenther, and G. E. Trahey, "Adaptive imaging and spatial compounding in the presence of aberration," *IEEE Trans. Ultrason., Ferroelectr., Freq. Control*, vol. 52, no. 7, pp. 1131–1144, Jul. 2005.

[25] S.-E. Måsøy et al., "Aberration correction in 2D echocardiography," *Quant. Imag. Med. Surg.*, vol. 13, no. 7, pp. 4603–4617, Jul. 2023. [Online]. Available: https://qims.amegroups.com/article/view/114222

[26] S. Li, W. N. McDicken, and P. R. Hoskins, "Refraction in Doppler ultrasound," *Ultrasound Med. Biol.*, vol. 19, no. 7, pp. 593–594, Jan. 1993. [Online]. Available: https://www.sciencedirect.com/science/article/pii/030156299390083Z

[27] D. A. Christopher, P. N. Burns, J. W. Hunt, and F. S. Foster, "The effect of refraction and assumed speeds of sound in tissue and blood on Doppler ultrasound blood velocity measurements," *Ultrasound Med. Biol.*, vol. 21, no. 2, pp. 187–201, Jan. 1995. [Online]. Available: https://www.sciencedirect.com/science/article/pii/S0301562994001014

[28] D. Zhao, L. N. Bohs, and G. E. Trahey, "Phase aberration correction using echo signals from moving targets I: Description and theory," *Ultrason. Imag.*, vol. 14, no. 2, pp. 97–110, Apr. 1992.

[29] L. Bohs, D. Zhao, and G. Trahey, "Phase aberration correction using echo signals from moving targets II: Experimental system and results," *Ultrason. Imag.*, vol. 14, no. 2, pp. 111–120, Apr. 1992.

[30] B.-F. Osmanski, G. Montaldo, and M. Tanter, "Aberration correction using moving particles speckle noise for ultrafast ultrasonic imaging," in *Proc. IEEE Int. Ultrason. Symp.*, Oct. 2010, pp. 983–986.

[31] B.-F. Osmanski, G. Montaldo, M. Tanter, and M. Fink, "Aberration correction by time reversal of moving speckle noise," *IEEE Trans. Ultrason., Ferroelectr., Freq. Control*, vol. 59, no. 7, pp. 1575–1583, Jul. 2012.

[32] N. M. Ivancevich, J. J. Dahl, G. E. Trahey, and S. W. Smith, "Phase-aberration correction with a 3-D ultrasound scanner: Feasibility study," *IEEE Trans. Ultrason., Ferroelectr., Freq. Control*, vol. 53, no. 8, pp. 1432–1439, Aug. 2006.

[33] N. M. Ivancevich, G. F. Pinton, H. A. Nicoletto, E. Bennett, D. T. Laskowitz, and S. W. Smith, "Real-time 3-D contrast-enhanced transcranial ultrasound and aberration correction," *Ultrasound Med. Biol.*, vol. 34, no. 9, pp. 1387–1395, Sep. 2008. [Online]. Available: https://www.sciencedirect.com/science/article/pii/S0301562908000367

[34] B. D. Lindsey, H. A. Nicoletto, E. R. Bennett, D. T. Laskowitz, and S. W. Smith, "3-D transcranial ultrasound imaging with bilateral phase aberration correction of multiple isoplanatic patches: A pilot human study with microbubble contrast enhancement," *Ultrasound Med. Biol.*, vol. 40, no. 1, pp. 90–101, Jan. 2014. [Online]. Available: https://www.sciencedirect.com/science/article/pii/S0301562913009885

[35] J. A. Jensen, "Field: A program for simulating ultrasound systems," *Med. Biol. Eng. Comput.*, vol. 4, no. 1, pp. 351–353, 1996.

[36] W. J. Davros, E. L. Madsen, and J. A. Zagzebski, "Breast mass detection by U.S.: A phantom study," *Radiology*, vol. 156, no. 3, pp. 773–775, Sep. 1985.

[37] L. Nock, G. E. Trahey, and S. W. Smith, "Phase aberration correction in medical ultrasound using speckle brightness as a quality factor," *J. Acoust. Soc. Amer.*, vol. 85, no. 5, pp. 1819–1833, May 1989.

[38] M. Hirama, O. Ikeda, and T. Sato, "Adaptive ultrasonic array imaging system through an inhomogeneous layer," *J. Acoust. Soc. Amer.*, vol. 71, no. 1, pp. 100–109, Jan. 1982, doi: 10.1121/1.387336.